Spatially homogeneous entanglement for matter-wave interferometry created with time-averaged measurements

Kevin C. Cox, Graham P. Greve, Baochen Wu, and James K. Thompson

Phys. Rev. A **94**, 061601 — Published 2 December 2016

DOI: 10.1103/PhysRevA.94.061601

Spatially Homogeneous Entanglement for Matter-Wave Interferometry Created with Time-Averaged Measurements

Kevin C. Cox, Graham P. Greve, Baochen Wu, and James K. Thompson
JILA, NIST, and Department of Physics, University of Colorado, 440 UCB, Boulder, CO 80309, USA

We demonstrate a method to generate spatially homogeneous entangled, spin-squeezed states of atoms appropriate for maintaining a large amount of squeezing even after release into the arm of a matter-wave interferometer or other free space quantum sensor. Using an effective intracavity dipole trap, we allow atoms to move along the cavity axis and time average their coupling to the standing wave used to generate entanglement via collective measurements, demonstrating 11(1) dB of directly observed spin squeezing. Our results show that time averaging in collective measurements can greatly reduce the impact of spatially inhomogeneous coupling to the measurement apparatus.

Spin-1/2 atoms must project into either "up" or "down" when measured. For N unentangled atoms, the independent randomness in this quantum projection fundamentally limits the single-shot phase resolution of any quantum sensor to $\Delta\phi_{\mathrm{SQL}} = 1/\sqrt{N}$ rad, the standard quantum limit (SQL) [1]. Collective measurements of atoms in optical cavities have recently produced some of the most strongly entangled, spin-squeezed states to date, directly improving the phase resolution of a quantum sensor's "clock hand" by a factor up to 60-70 (roughly 18 dB) in noise variance below the SQL [2, 3].

Spin-squeezed states could be used to improve a wide range of quantum sensors, with today's best atomic clocks [4–6] being particularly promising candidates [7, 8]. In this work we focus on preparing spin-squeezed states appropriate for matter-wave atom interferometry with applications including inertial sensing [9], measurements of gravity and freefall, [10, 11] and even the search for certain proposed types of dark matter and dark energy [12, 13].

A major challenge arises for cavity-based atom interferometry and other applications involving release of spin-squeezed atoms into free space. The problem is that the probe mode used to perform the collective measurement is a standing wave, but the atoms are trapped in a 1-dimensional lattice defined by a standing wave cavity mode with a significantly different wavelength. Some atoms will sit in lattice sites positioned near nodes and some near anti-nodes of the entanglement-generating probe light. As a result, the atoms will contribute to the collective measurement with different strengths. In this common case, the large degree of squeezing exists only for this specific coupling configuration and would be largely lost after releasing the atoms into the arm of an interferometer, since their final coupling to the cavity mode or other readout detector will be different from the original configuration [14]. In contrast, we wish to create spatially homogeneous entanglement, quantified by the amount of observed phase resolution beyond the SQL that one can achieve when every atom couples equally to the final measurement apparatus.

In this Letter, we demonstrate a method to create homogeneous spin-squeezed states in a standing wave optical cavity by allowing the atoms to traverse many wavelengths of the standing wave during each collective measurement. Atoms experience a time-averaged coupling to the cavity so that every atom is measured with the same strength, ensuring homogeneous entanglement. We do this by creating an optical trap with a uniform axial potential, which we refer to as an effective "dipole trap" as opposed to the standing-wave "lattice". The dipole

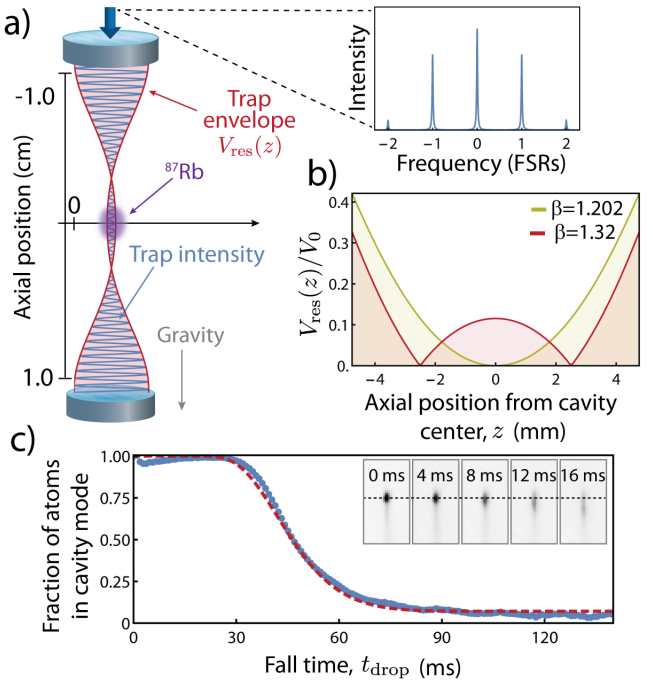

FIG. 1. (a) Optical lattice sidebands separated by one free spectral range (FSR) are injected into the cavity to create an axially homogeneous "dipole" trap. The dipole trap intensity and its envelope are plotted inside of the optical cavity, with exaggerated wavelength $\lambda_l \times 10^3$. (b) The envelope of the residual lattice potential $V_{\mathrm{res}}(z)$ normalized to the peak lattice potential depth V_0 is plotted near the cavity center, optimized for a minimum at $z = 0$ (gold, $\beta = 1.20$) and for the minimal fraction of trapped atoms determined experimentally (red, $\beta = 1.32$). (c) Fraction of atoms remaining in the cavity mode (blue points) vs. fall time, fit to a model (red dash) described in the text. Fluorescence images show the falling atom cloud at various times (inset).

trap maintains transverse confinement of the atoms while allowing free movement subject to gravity along the vertical cavity axis. We demonstrate 11(1) dB of directly observed squeezing via collective measurements in the dipole trap and use fluorescence images and noise scalings to show that the generated squeezing is homogeneously shared among the atoms to a large degree, in principle allowing significant amounts of squeezing for free space or guided matter-wave interferometry. We also discuss the limits placed on entanglement generation with time-averaged measurements.

Homogeneous squeezing can also be obtained using a travelling wave "ring" cavity [15], but birefringence must be controlled to maintain the efficacy of utilizing cycling transitions [16]. Another appealing approach is to introduce a commensurate lattice [3, 17]. This approach requires special mirror coatings and frequency doubling equipment and doesn't permit guided movement for atom interferometry within the cavity mode. Homogeneous entangled states can also be obtained without using a cavity [18–22], but free space experiments have not yet achieved the large amounts of squeezing observed using optical cavities.

In this work, we use the pseudo-spin states defined by the ground hyperfine states of ^{87}Rb, with $|\downarrow\rangle \equiv |5^2S_{1/2}, F = 1, m_F = 1\rangle$ and $|\uparrow\rangle \equiv |5^2S_{1/2}, F = 2, m_F = 2\rangle$ split by 6.8 GHz. As in Refs. 2 and 16, we describe the total pseudo-spin state of N atoms by a collective Bloch vector $\vec{J}$, with spin projections J_x, J_y, and J_z. The spin projection on a single trial $J_z = N_\uparrow - \frac{N}{2}$ is determined by making a collective measurement of the total number of atoms in the upper spin state $N_\uparrow$. For an unentangled, coherent spin state (CSS), quantum projection noise (QPN) leads to fluctuations in J_z of size $\Delta J_{z,\mathrm{QPN}} = \sqrt{N}/2$. In this work, ΔX will refer to the standard deviation of a quantity X as measured over repeated trials of the experiment.

The collective measurement is performed using the experimental apparatus and techniques described in Ref. 2. In brief, we trap ^{87}Rb atoms in the central 2 mm of a 2 cm optical cavity with finesse $F = 2532(80)$. A cavity mode is tuned $\delta_c = 2\pi \times 400$ MHz to the blue of the $|\uparrow\rangle$ to $|e\rangle \equiv |5^2P_{3/2}, F = 3, m_F = 3\rangle$ transition. The cavity resonance frequency ω is shifted by an amount depending on the number of atoms in $|\uparrow\rangle$ due to the dispersive interaction between the atoms and cavity. The cavity's resonance frequency is measured by probing the cavity in reflection for 40 μs. The probing is collective because it is not possible to tell from the single probe mode precisely which atoms are in $|\uparrow\rangle$.

In a single trial, we apply resonant microwaves to prepare each atom in an equal superposition $(|\uparrow\rangle + |\downarrow\rangle)/\sqrt{2}$. We then perform two consecutive measurements of the projection J_z, with the two measurement outcomes labeled J_{zp} and J_{zf}, with subscripts denoting pre and final measurement. The quantum projection noise is common to the two measurements and is removed when we take the difference between the pre and final measurements, yet the atoms nearly completely retain coherence of the quantum phase between $|\uparrow\rangle$ and $|\downarrow\rangle$. This allows one to sense a quantum phase that evolves between the final and premeasurements below the SQL.

The atoms are initially cooled to approximately 10 μK and trapped in a far off resonance red detuned optical lattice at $\lambda_l = 823$ nm (with corresponding wave vector $k_0 = 2\pi/\lambda_l$). We then convert this standing-wave lattice into an effective dipole trap. This is achieved by simultaneously driving multiple TEM_{00} longitudinal modes of the cavity near 823 nm. Adjacent longitudinal modes have opposite symmetry with respect to the cavity center. To lowest order, near the center of the cavity, one mode creates a $\cos^2(k_0 z)$ standing-wave intensity profile while the next mode creates a $\sin^2(k_0 z)$ intensity profile such that the sum of the two standing waves $\cos^2(k_0 z) + \sin^2(k_0 z) = 1$ creates a net uniform intensity profile along the cavity axis as shown in Fig. 1(a).

To drive adjacent longitudinal modes, we phase modulate the lattice light at the cavity free spectral range (FSR), FSR $= 2\pi \times 8.1050(5)$ GHz, using a fiber-coupled phase modulator. The resulting axial component of the potential at distance z from the cavity center can be written $V(z) = V_0[J_0^2(\beta)\cos^2(k_0 z) + J_{-1}^2(\beta)\sin^2((k_0 + \delta k_{-1})z) + J_1^2(\beta)\sin^2((k_0 + \delta k_1)z) + \dots]$, where $J_n(\beta)$ is the nth Bessel function and β is the modulation index. $\delta k_n = n\mathrm{FSR}/c$ is the additional wave vector for the sidebands offset by n cavity free spectral ranges, with speed of light c. Interference terms between sidebands are neglected since they oscillate at 8 GHz.

Figure 1(b) shows the depth of the residual standing-wave lattice potential in the dipole trap $V_{\mathrm{res}}(z)$ as a function of distance from the center of the cavity for two different values of β. We find $\beta \approx 1.32$ (overdriving the dipole trap) to be the optimum value for freeing atoms to move. This is due to a wider minimum of $V_{\mathrm{res}}(z)$ which overlaps the atomic spatial distribution as well as the fact that overdriving causes the lattice potential wells to be converted into small potential peaks, giving atoms additional potential energy.

When an atom begins to fall in the dipole trap, the increase in the residual lattice depth is not sufficient to stop the atom from continuing to fall; rather, we expect the atom to be guided by the optical dipole trap until it collides with the lower mirror. In Fig. 1(c), we measure the number of atoms in the cavity as a function of freefall time, t_{drop}, by continuously monitoring the dispersive shift of the cavity resonance frequency. The data is renormalized to account for background atom loss and is reasonably described by a fit (purple line) which assumes atoms are guided by the net transverse intensity profile of the dipole trap until they are lost when they collide with the lower mirror. For comparison, ballistic expansion out of the cavity mode would occur in only 2 ms if we were to simply turn off the optical lattice. The free fall and guiding are corroborated by fluorescence measurements such as shown in Fig. 1(c) inset for various t_{drop}. Figure 1(c) and fluorescence images indicate that

at long times only 5(1)% of the atoms remain trapped due to the spatial extent of the cloud and the small resudual lattice. The majority of the atoms move along the cavity axis, the key for obtaining time-averaged homogeneity in the coupling of the atoms to the standing-wave probe mode.

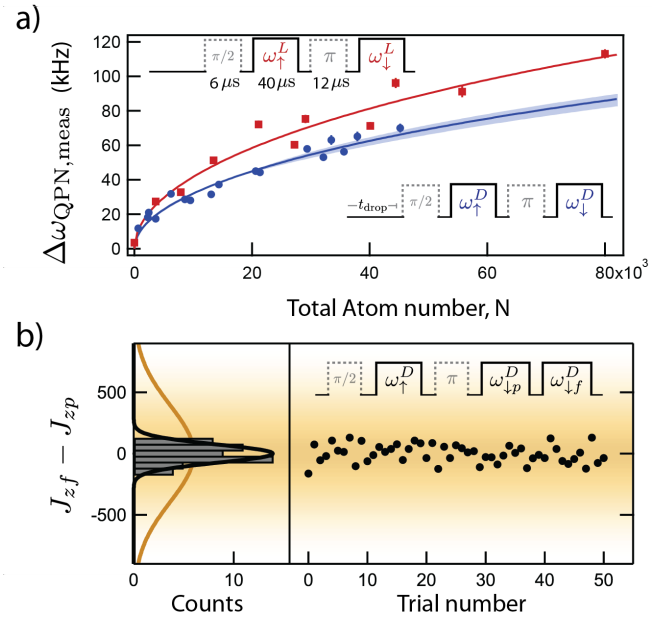

FIG. 2. (a) Projection noise scaling versus total atom number N, measured in the lattice (red squares) including a theoretical prediction (red line) and in the dipole trap (blue circles) including a fit to infer a coupling fraction ζ (blue line, with 68% confidence interval bands). Sequences are inset. Durations of microwave pulses and measurements are shown in the first sequence. Dashed boxes represent Bloch vector rotations through a given angle using resonant microwaves. Solid boxes represent cavity frequency measurements. (b) Quantum noise reduction in the dipole trap with $6.3(3)\times10^5$ atoms. A histogram of $J_{zf} - J_{zp}$ (black data points) shows a standard deviation 13.9(6) dB below projection noise $\Delta J_{z,\mathrm{QPN}} = 397$ atoms (gold line and shaded distribution). The measurement sequence is inset.

For a fixed total atom number, we expect the projection noise induced fluctuations in the cavity resonance frequency $\Delta\omega_{\mathrm{QPN}}$ to be smaller in the dipole trap than in the lattice. While the total dispersive shift is the same in both cases, in the lattice the dominant contribution is from the subset of atoms situated near antinodes of the probe. The ith atom's coupling to the cavity is defined by its Jaynes-Cummings coupling parameter g_i, with a single-photon Rabi frequency given by $2g_i$. The atoms at antinodes have a coupling g_i near the maximum value $g_0 = 2\pi \times 0.519(5)$ MHz and provide stronger than average fluctuations in the cavity resonance frequency. In the ideal time-averaged situation, on the other hand, the full ensemble only couples with the rms coupling strength $g_{rms} = g_0/\sqrt{2}$, actually leading to weaker cavity frequency fluctuations. To quantify the level of homogeneous coupling, we define a model where fractionally, ζ of the atoms release into the dipole trap and are assumed to have perfectly homogeneous coupling. $1-\zeta$ of the atoms remain fixed in position and maintain their original coupling. In this model, the projection noise induced fluctuations in the cavity resonance frequency can be written $\Delta\omega_{\mathrm{QPN}} = g_{\mathrm{rms}}^2\sqrt{N(3-\zeta)}/\sqrt{8(g_0^2N+\delta_c^2)}$ [23].

We observe this change in the projection noise scaling between the lattice and dipole trap by performing the measurement sequences of Fig. 2(a) in the lattice (red, superscript L) and in the dipole trap (blue, superscript D) versus the total atom number in the cavity N. The $\omega_\uparrow$ and $\omega_\downarrow$ windows represent the outcome of a measurement of the cavity resonance frequency, sensitive to $N_\uparrow$ or $N_\downarrow$ respectively, and we plot the observed projection noise fluctuations $\Delta\omega_{\mathrm{QPN,meas}} = \Delta(\omega_\uparrow - \omega_\downarrow)$ in either the lattice or the dipole trap. The lattice data is used as a calibration of g_0 with the theoretical scaling plotted in red. The dipole trap data is fit to the model $2 \times \Delta\omega_{\mathrm{QPN}}$ (since the measurement sequence includes two anti-correlated windows, $\omega_\uparrow$ and $\omega_\downarrow$) with ζ as a free parameter. We fit $\zeta = 1.0(2)$, consistent with our expectation of 95% from the data in Fig. 1(c). In both the lattice and dipole data of Fig. 2(a), a small linear contribution to $\Delta\omega_{\mathrm{QPN,meas}}$ (as opposed to $\Delta\omega_{\mathrm{QPN}} \propto \sqrt{N}$), due to noise in the π-pulse, is observed and included in the fit model. For simplicity, this contribution has been subtracted from both the data and fit in Fig. 2(a).

By consecutively performing a pre and final measurement $\omega_\downarrow^{\mathrm{D}}$, labeled $\omega_{\downarrow p}^{\mathrm{D}}$ and $\omega_{\downarrow f}^{\mathrm{D}}$ we can show a large degree of spin noise reduction below QPN and correspondingly demonstrate the creation of entangled, spin-squeezed states in the dipole trap. We measure spin squeezing using the Wineland criterion for phase enhancement relative to the SQL, $(\Delta\theta/\Delta\theta_{\mathrm{SQL}})^2 \equiv S = R/C^2$ [2, 24]. The observed spin noise reduction normalized to the quantum projection noise level is $R = (\Delta(J_{zf} - J_{zp})/\Delta J_{z,\mathrm{QPN}})^2 < 1$. Squeezing or enhanced phase resolution also requires the additional demonstration of retained coherence, or Bloch vector length, often referred to as "contrast", $C \equiv 2|\vec{J}|/N$.

The measurement sequence is shown in the inset of Fig. 2(b) and is the same as that of Ref. [2]. We use $t_{\mathrm{drop}} = 13$ ms, which accelerates the atoms enough to average over approximately 13 cycles of the probe standing wave during the 40 μs measurement window. Figure 2(b) shows noise in measurements of $\omega_{\downarrow f}^{\mathrm{D}} - \omega_{\downarrow p}^{\mathrm{D}}$ in the dipole trap with total atom number $N = 630(30) \times 10^3$ atoms. Experimental parameters g_{rms}, δ_c, and N are used to scale between cavity frequency measurements and J_z, $\partial\omega/\partial J_z = g_{rms}^2/\sqrt{4g_{rms}^2N_\uparrow + \delta_c^2}$. The data is collated into a histogram on the left, showing a standard deviation 13.9(6) dB less than the projection noise level shown in yellow. No noise subtractions or postselection were applied to data in which squeezing is observed. The remaining contrast after the premeasurement was independently measured, C =0.70(5). Together with the noise reduction, this yields a directly observed phase res-

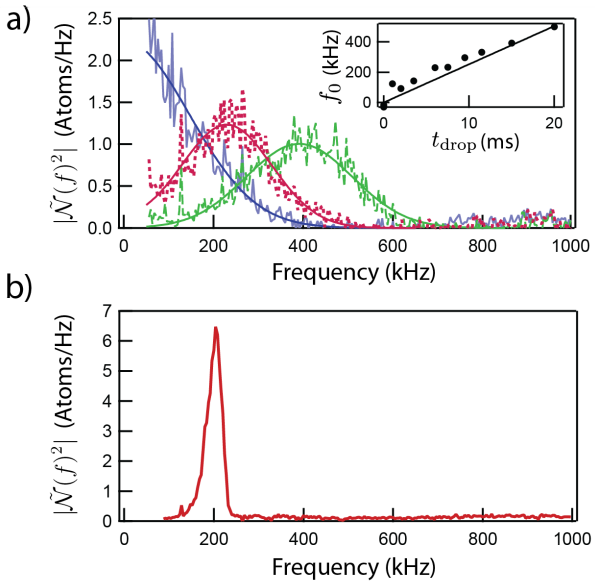

FIG. 3. (a) Power spectra showing coupling oscillations for fall times of 1 ms (blue solid), 7.5 ms (red dotted) and 15 ms (green dashed) with their respective fits. (inset) Center frequency f_0 of the fitted Boltzmann distribution for various fall times (points) compared to a freefall prediction line of $f_0 = 2at/\lambda_p$ (line), see text for definitions. (b) Power spectrum showing coupling oscillations at the trap frequency when atoms are trapped in the optical lattice.

olution, or spin squeezing, of $S = 1/13(3)$ or $-11(1)$ dB below the SQL

When the cavity frequency is measured in a 40 μs window using the dipole trap, oscillations in the signal are observed, indicating the atomic motion over the probe standing wave. Specifically, we measure the number of atoms $N_\uparrow$ that are coupled to the cavity as a function of time by applying a scale factor to convert cavity frequency to atom number. We refer to this rescaled time signal as $\mathcal{N}(t) = \sum_i^{N_\uparrow} g_i^2(t)/g_{\rm rms}^2$. We observe noise in the atom's coupling in the frequency domain, which can be used to infer the distribution of atoms' coupling oscillation frequencies. Most of the coupling oscillations average away, since the oscillation of each atom occurs with a random phase. However, the residual uncancelled coupling oscillations are observed in $\mathcal{N}(t)$ such that the squared Fourier transform of the time signal, $|\tilde{\mathcal{N}}(f)^2|$ has units of Atoms/Hz and is closely related to the atomic velocity distribution.

Figure 3(a) shows $|\tilde{\mathcal{N}}(f)^2|$, recorded using 2 ms of data and taking the average power spectrum of time traces from approximately 65 trials. The data was taken after 1 ms (blue), 7.5 ms (red), and 15 ms (green) of freefall time after release into the dipole trap. Each power spectrum is fit to an appropriately folded 1D Boltzmann distribution that accounts for the inability to distinguish between upwards and downwards velocities. The fit center frequency f_0 is plotted as a function of the freefall time t in the inset of Fig. 3(a). The result is consistent, particularly at long times, with the simple prediction, $f_0 = a\,t/(\lambda_p/2)$, where $a = 9.81$ m/s^2 is the acceleration due to gravity. The widths of the distributions are consistent with Boltzmann distributions giving final axial temperatures of 25 μK. To contrast, Fig. 3(b) shows $|\tilde{\mathcal{N}}(f)^2|$ for atoms in the lattice. Instead of a large thermal distribution, a narrow distribution is observed at the lattice trap frequency, about 200 kHz.

In summary, we infer that we have created a spatially homogeneous squeezed state from the combined observations of Figs. 1-3. First, we observe release of 95(1)% of the atoms (Fig. 1) at a sufficient velocity (Fig. 3) to ensure, on average, 13 averaging cycles of the probe standing wave during a 40 μs collective measurement. In Fig. 2(a) we also confirm the transformation to homogenous coupling by the change in scaling of projection noise fluctuations of the cavity. The demonstration of 11(1) dB of observed squeezing in the homogeneous configuration proves our ability to create a large amount of entanglement in this highly time-averaged scheme.

We derive in detail various theoretical limits to our time-averaging technique in the Supplemental Material [23]. These calculations may be useful for future implementations of time averaging in various types of atom interferometers or other free space sensors. However, we emphasize that since our experimental results demonstrate, apart from Refs. 2 and 3, the largest ever directly-observed atomic entanglement enhancement, our data already establishes this method as useful for generating large amounts of homogeneous spin squeezing. We summarize a few limitations to time-averaged squeezing in the following paragraph.

Since the ac signals in Fig. 3 yield additional information about the spin state of each velocity component of the atomic ensemble, time averaging will fundamentally limit the squeezing to order $S \propto \frac{1}{qN}$, where q is the total quantum efficiency of the experiment. For $q \sim 1$, this is close to the Heisenberg limit. A more relevant limitation for our system is imperfect averaging of the probe standing wave. For 40 μs measurements after a 13 ms drop time and for a 25 μK ensemble, we estimate that the observed noise reduction should be limited to 15 dB below QPN, which we believe to be a primary limitation to our observed spin noise reduction of 13.9(6) dB. In the future, this limit could be improved using longer measurement windows or drop times to average over more cycles of the probe standing wave during each measurement. The noise reduction limit due to imperfect time averaging improves as $R \propto 1/(T_{\rm win}^2 T_{\rm drop}^2)$ [23] for a freefall duration of $T_{\rm drop}^2$ measurement windows with duration $T_{\rm win}$.

To realize a free space matter-wave interferometer, atoms could be prepared in the cavity for the entanglement generating premeasurement, then released into free space for an interferometry sequence. Large momentum transfers, similar to Ref. 25, could in principle be used to separate the wavefunction by a large distance. The final measurement could be performed with fluorescence

detection at any location. The 5% of atoms with non-uniform coupling during the premeasurement would lead to an additional noise floor, not observed in this work, of 13 dB below the SQL. Additionally, inhomogeneity from radial motion will lead to another additional noise floor of approximately 10 dB below the SQL [2]. Notably, this radial motion would also equally affect systems using ring cavities, commensurate lattices, or other axial averaging techniques. For this reason, we do not expect our time averaging scheme to have significant fundamental advantages or disadvantages for free space interferometry compared to recent results with a commensurate lattice [3, 17].

Another possibility is to perform guided interferometry inside the cavity mode. Here the pre and final measurements would both be performed with collective cavity measurements. In this case, the noise from the 5% of atoms remaining trapped in the residual lattice and radial motion largely cancels at short times. The 11(1) dB of squeezing observed in this work would in principle fully translate to this type of interferometer. In addition to the possibility of using entangled states, performing the final readout via a cavity measurement may allow for reduced technical noise, higher bandwidth, cleaner optical modes, and power buildup for Raman transitions [26]. For the current system the maximum free-fall evolution time of this interferometer would be limited to approximately 50 ms due to the 2 cm long cavity. Additionally, the optical potential from the residual lattice corrugation may cause small erroneous signals in an atom interferometer sequence. However, these signals could be sufficiently reduced using larger optical cavities or more frequency components to create a more perfect effective dipole trap with smaller residual lattice corrugation.

Additionally, in concert with this method, higher order transverse modes, atom-chip technologies [27, 28], or tailored potentials [29, 30] might be combined with the cavity measurement technique presented here to create new varieties of matter-wave Sagnac interferometers and other inertial sensors. The real-time observation of mechanical motion also opens the path to stochastic cooling schemes based on measurement and feedback [31] with applications to more complex systems such as molecules, which can be challenging to laser cool using conventional Doppler cooling methods.

We gratefully acknowledge support from NIST, DARPA QuASAR, ARO, and NSF PFC. This material is based upon work supported by the National Science Foundation under Grant Number 1125844 Physics Frontier Center.

[1] W. M. Itano, J. C. Bergquist, J. J. Bollinger, J. M. Gilligan, D. J. Heinzen, F. L. Moore, M. G. Raizen, and D. J. Wineland, Physical Review A **47**, 3554 (1993).
[2] K. C. Cox, G. P. Greve, J. M. Weiner, and J. K. Thompson, Phys. Rev. Lett. **116**, 093602 (2016).
[3] O. Hosten, N. J. Engelsen, R. Krishnakumar, and M. A. Kasevich, Nature **529**, 505 (2016).
[4] T. Nicholson, S. Campbell, R. Hutson, G. Marti, B. Bloom, R. McNally, W. Zhang, M. Barrett, M. Safronova, G. Strouse, *et al.*, Nature communications **6** (2015).
[5] N. Hinkley, J. Sherman, N. Phillips, M. Schioppo, N. Lemke, K. Beloy, M. Pizzocaro, C. Oates, and A. Ludlow, Science **341**, 1215 (2013).
[6] I. Ushijima, M. Takamoto, M. Das, T. Ohkubo, and H. Katori, Nature Photonics **9**, 185 (2015).
[7] M. A. Norcia and J. K. Thompson, Phys. Rev. A **93**, 023804 (2016).
[8] E. S. Polzik and J. Ye, Phys. Rev. A **93**, 021404 (2016).
[9] B. Barrett, A. Bertoldi, and P. Bouyer, Physica Scripta **91**, 053006 (2016).
[10] G. Rosi, F. Sorrentino, L. Cacciapuoti, M. Prevedelli, and G. M. Tino, Nature **510**, 518 (2014).
[11] D. Schlippert, J. Hartwig, H. Albers, L. L. Richardson, C. Schubert, A. Roura, W. P. Schleich, W. Ertmer, and E. M. Rasel, Phys. Rev. Lett. **112**, 203002 (2014).
[12] C. J. Riedel, Phys. Rev. D **88**, 116005 (2013).
[13] P. Hamilton, M. Jaffe, P. Haslinger, Q. Simmons, H. Müller, and J. Khoury, Science **349**, 849 (2015).
[14] J. Hu, W. Chen, Z. Vendeiro, H. Zhang, and V. Vuletić, Phys. Rev. A **92**, 063816 (2015).
[15] S. Bernon, T. Vanderbruggen, R. Kohlhaas, A. Bertoldi, A. Landragin, and P. Bouyer, New Journal of Physics **13**, 065021 (2011).
[16] Z. Chen, J. G. Bohnet, J. M. Weiner, K. C. Cox, and J. K. Thompson, Phys. Rev. A **89**, 043837 (2014).
[17] J. Lee, G. Vrijsen, I. Teper, O. Hosten, and M. A. Kasevich, Optics letters **39**, 4005 (2014).
[18] C. Gross, T. Zibold, E. Nicklas, J. Estve, and M. K. Oberthaler, Nature **464**, 1165 (2010).
[19] J. Appel, P. Windpassinger, D. Oblak, U. Hoff, N. Kjærgaard, and E. Polzik, Proc. Natl. Acad. Sci. **106**, 10960 (2009).
[20] N. Behbood, F. Martin Ciurana, G. Colangelo, M. Napolitano, G. Tóth, R. J. Sewell, and M. W. Mitchell, Phys. Rev. Lett. **113**, 093601 (2014).
[21] W. Muessel, H. Strobel, D. Linnemann, D. B. Hume, and M. K. Oberthaler, Phys. Rev. Lett. **113**, 103004 (2014).
[22] C. D. Hamley, C. S. Gerving, T. M. Hoang, E. M. Bookjans, and M. S. Chapman, Nat. Phys. **8**, 305 (2012).
[23] See Supplemental Material which includes Refs. [32–36] for a derivation of squeezing limits with inhomogeneous coupling and a discussion of the limits to spin squeezing using time averaging.
[24] D. J. Wineland, J. J. Bollinger, W. M. Itano, F. L. Moore, and D. J. Heinzen, Phys. Rev. A **46**, R6797 (1992).
[25] T. Kovachy, P. Asenbaum, C. Overstreet, C. Donnelly, S. Dickerson, A. Sugarbaker, J. Hogan, and M. Kasevich, Nature **528**, 530 (2015).
[26] P. Hamilton, M. Jaffe, J. M. Brown, L. Maisenbacher, B. Estey, and H. Müller, Phys. Rev. Lett. **114**, 100405 (2015).
[27] Y.-J. Wang, D. Z. Anderson, V. M. Bright, E. A. Cornell, Q. Diot, T. Kishimoto, M. Prentiss, R. A. Saravanan,

S. R. Segal, and S. Wu, Phys. Rev. Lett. **94**, 090405 (2005).
[28] S. Wu, E. Su, and M. Prentiss, Phys. Rev. Lett. **99**, 173201 (2007).
[29] V. Guarrera, R. Szmuk, J. Reichel, and P. Rosenbusch, New Journal of Physics **17**, 083022 (2015).
[30] I. Lesanovsky and W. von Klitzing, Phys. Rev. Lett. **99**, 083001 (2007).
[31] V. Vuletić, J. K. Thompson, A. T. Black, and J. Simon, Phys. Rev. A **75**, 051405 (2007).
[32] M. H. Schleier-Smith, I. D. Leroux, and V. Vuletić, Phys. Rev. Lett. **104**, 073604 (2010).
[33] J. G. Bohnet, K. C. Cox, M. A. Norcia, J. M. Weiner, Z. Chen, and J. K. Thompson, Nat. Photon. **8**, 731 (2014).
[34] I. D. Leroux, M. H. Schleier-Smith, and V. Vuletić, Phys. Rev. Lett. **104**, 073602 (2010).
[35] Z. Chen, J. G. Bohnet, S. R. Sankar, J. Dai, and J. K. Thompson, Phys. Rev. Lett. **106**, 133601 (2011).
[36] F. Marquardt, J. P. Chen, A. A. Clerk, and S. M. Girvin, Phys. Rev. Lett. **99**, 093902 (2007).